Petroleum Science
https://doi.org/10.1007/s12182-021-00555-0

ORIGINAL ARTICLE

Modeling the effects of fracture infill on frequency-dependent anisotropy and AVO response of a fractured porous layer

Yan-Xiao He[1] · Xin-Long Li[1] · Gen-Yang Tang[1] · Chun-Hui Dong[1] · Mo Chen[2] · Shang-Xu Wang[1]

Received: 2 November 2020 / Accepted: 12 December 2020

Abstract

In a fractured porous hydrocarbon reservoir, wave velocities and reflections depend on frequency and incident angle. A proper description of the frequency dependence of amplitude variations with offset (AVO) signatures should allow effects of fracture infills and attenuation and dispersion of fractured media. The novelty of this study lies in the introduction of an improved approach for the investigation of incident-angle and frequency variations-associated reflection responses. The improved AVO modeling method, using a frequency-domain propagator matrix method, is feasible to accurately consider velocity dispersion predicted from frequency-dependent elasticities from a rock physics modeling. And hence, the method is suitable for use in the case of an anisotropic medium with aligned fractures. Additionally, the proposed modeling approach allows the combined contributions of layer thickness, interbedded structure, impedance contrast and interferences to frequency-dependent reflection coefficients and, hence, yielding seismograms of a layered model with a dispersive and attenuative reservoir. Our numerical results show bulk modulus of fracture fluid significantly affects anisotropic attenuation, hence causing frequency-dependent reflection abnormalities. These implications indicate the study of amplitude versus angle and frequency (AVAF) variations provides insights for better interpretation of reflection anomalies and hydrocarbon identification in a layered reservoir with vertical transverse isotropy (VTI) dispersive media.

Keywords Seismic anisotropy · Fractured media · Attenuation and dispersion · AVO responses · Frequency dependence

1 Introduction

Quantitative analysis of seismic reflections suggests that hydrocarbon-bearing regions often show anomalously high levels of wave attenuation and the associated strong dispersion of phase velocity (e.g., Brajanovski et al. 2010; Cao et al. 2016; Carcione and Picotti 2006; Deng et al. 2020; Gurevich et al. 2010; Li et al. 2020; Rubino and Holliger 2013; Wu et al. 2014; Zhang et al. 2017). The resulted effect on seismic reflection signatures, however, this has not been considered accurately during the traditional AVO response analysis. Numerous researchers have employed the Biot's poroelastic theory (Biot 1962a, b) to investigate the behaviors of reflected and transmitted waves from an interface separating two poroelastic layers filled with different fluids. The classic Biot's theory, unfortunately, underestimates substantially the wave attenuation; it yields negligible attenuation in the seismic-exploration band. Nevertheless, larger than usual levels of attenuation can be predicted when considering heterogeneous media, such as partial saturation and fractured porous medium. Meanwhile, the fractured reservoir systems are important for the storage of underground water and monitoring of the injected carbon dioxide. And thus, an appropriate characterization of natural fractures using surface seismic observations may potentially provide significant implications for an improved calculation of pore-fluid flow patterns and media permeability within a fractured poroelastic reservoir (e.g., Maultzsch et al. 2003; Chapman et al. 2006; Guo et al. 2018; Zhang et al. 2018; Cao et al. 2019; Guo et al. 2019).

Edited by Jie Hao and Chun-Yan Tang.

✉ Shang-Xu Wang
wangsx@cup.edu.cn

[1] State Key Laboratory of Petroleum Resources and Prospecting, CNPC Key Laboratory of Geophysical Exploration, China University of Petroleum (Beijing), Beijing 102249, China

[2] Daqing Oilfield Exploration and Development Institute, Daqing 163000, Heilongjiang Province, China

Published online: 19 May 2021

The philosophy that we hope to develop in this study holds that strong wave attenuation and the associated velocity dispersion anomaly is the measured ground truth and we should, therefore, focus our attention on those physical mechanisms. Using the more specific mechanism, the existence of excess attenuation and dispersion of phase velocity related to the hydrocarbon-bearing regions can be interpreted with enhanced confidence.

It is broadly accepted that periodically stratified rocks show important VTI anisotropic property and are widely distributed within the crust. Previous authors have made plenty of attempts to determine the frequency-dependent anisotropy considering wave attenuation and dispersion of phase velocity due to the squirt flow mechanism (Chapman 2003; Tang 2011), as well as the mesoscopic flow effect (e.g., Krzikalla and Muller 2011; Carcione et al. 2013; Kudarova et al. 2013; Galvin and Gurevich 2015). Researchers have also addressed the sensitivity of reservoir acoustic properties to the fracture size, fracture weakness and facture infills (e.g., Maultzsch et al. 2003; Chichinina et al. 2006; Rubino et al. 2016; Shi et al. 2018). However, how the anisotropic poroelasticities of fractured porous layers affect the frequency-dependent seismic AVO response signatures, to the authors' knowledge, has not been fully investigated. In addition, current analysis on seismic AVO signatures normally uses single interface reflection model or normal-incidence reflection approach. This forward modeling has not accurately considered the influences of both the stratified structure and the attenuation and dispersion of complex stiffness tensors from rock physics simulation in the computations of angle- and frequency-dependent reflection coefficients (e.g., Rüger et al. 1997; Ren et al. 2009; Liu et al. 2011; Dupuy and Stovas 2014a, b; Zhao et al. 2015; Kumari et al. 2017; Kumar et al. 2018; He et al. 2019).

Recent studies have demonstrated that wave attenuation and velocity dispersion may produce important influences on seismic AVO analysis in fractured porous reservoirs (e.g., Guo et al 2015a, b; Guo et al 2016, 2017a, b). Nevertheless, few publications deal with the means to quantitatively explore the seismic AVAF response anomalies of an anisotropic medium, particularly for the anisotropy variations as a function of frequency. To the best of our knowledge, Chapman et al. (2006) have first introduced a methodology that was utilized to evaluate the influences of abnormally high values of velocity dispersion and attenuation from the fluid-filled reservoir on seismic measurements. In their presented work, seismic reflections at an interface between a nondispersive overburden and an equivalent dispersive layer were obtained using a reflectivity technique. Additionally, based on Brajanovski's porous and fractured model (Brajanovski et al. 2005), Yang et al. (2017) examined the characteristics of seismic responses from an interface separating a purely elastic isotropic overburden and a dispersive sandstone having weak to moderate velocity anisotropy. Via using a generalized Zoeppritz equation-based method, Jin et al. (2018) explored the impacts of anisotropic attenuation and velocity dispersion on P-wave reflection signatures and observed that fracture-related anisotropic velocity dispersion can substantially affect both the magnitude and phase variations of P-wave reflections as expected.

In what follows we study first the effects of fracture infills on angle- and frequency-dependent elastic properties of a porous medium permeated by sets of aligned fractures. And then we investigate numerically the influences of abnormally high levels of wave attenuation and velocity dispersion on seismic reflection signatures. In this study, the effect of velocity dispersion and attenuation was determined using an equivalent effective medium theory based on the mesoscopic wave-induced fluid flow concept of Norris (1993) (please also read Brajanovski et al. 2005; Kong et al. 2017) for fractured porous rocks, in which the pores and fractures are filled with two different fluids. Using a frequency-domain propagator matrix algorithm that allows anisotropic elastic tensors, in this presented work we perform our calculations of seismic AVO responses from a hydrocarbon reservoir with complex lithology (Guo et al. 2015a, b; He et al. 2018). The numerically modeling results demonstrate that the frequency-dependent responses are closely related to seismic AVO signatures in an interbedded reservoir system and hence a potential effective approach to help to identify fracture-filled fluid variations inside an interbedded porous reservoir.

2 Methodology

2.1 Anisotropic wave attenuation and velocity dispersion in a fluid-saturated fractured poroelastic medium

Although the geometries of rock fractures are very complex, they can be represented by highly porous permeable layers which are also noted as planer fractures, in case the fracture radii are much smaller than the fracture spacing and seismic wavelengths. Thus, the porous rock having a set of aligned planer fractures can be treated as a layered poroelastic medium with infinite extents in lateral. Plenty of rock physics theories that have been derived specifically to explore the frequency dependence in the elastic stiffness tensors press the main challenges in carrying out seismic AVO modeling analysis, principally porosity–anisotropic velocity transform, velocity–pressure relation, fluid saturation and velocity prediction. In this study, an extended poroelastic theory based on Carcione et al. (2013) and Kong et al. (2017) was utilized for the determination of frequency-dependent full elastic stiffness tensors. Additionally, the introduced theory allows

us to account for fluid-sensitive attenuation and velocity dispersion attributes in the frame of anisotropic viscoelasticity.

On the basis of the assumption that waves propagating is always normal to the layering plane, all interlayer flow models can be approximated using an unrelaxed (high-frequency) and a relaxed (low-frequency) P-wave stiffness value related by a frequency-dependent function (i.e., Krzikalla and Müller 2011; Carcione et al. 2013). For wave propagation in a fractured poroelastic medium that is simulated as a periodically stratified system of two different layers as described above, we compute the complex and frequency-dependent VTI stiffnesses C_{ij} according to the poroelastic Backus averaging based on the equation

$$C_{ij} = C_{ij}^{\text{high}} - R(\omega) \cdot \left(C_{ij}^{\text{high}} - C_{ij}^{\text{low}} \right) \tag{1}$$

where ω is the angular frequency ($=2\pi f$), and the subscript pair *(ij)* indicates (11), (13), (33), (44) and (66), respectively. The scalar complex relaxation function *R(ω)* can be obtained through normalizing the normal-incidence P-wave stiffness C_{33} with its relaxed and unrelaxed limits as

$$R(\omega) = \frac{C_{33} - C_{33}^{\text{high}}}{C_{33}^{\text{low}} - C_{33}^{\text{high}}} \tag{2}$$

With Eq. (1), we derive all effective stiffness components, and the anisotropic properties are determined fully by the high-frequency and low-frequency limits C_{33}^{high} and C_{ij}^{low}. The frequency dependence of the elastic stiffnesses C_{ij} is controlled solely by the scalar complex relaxation function *R(ω)*. In such a medium, attenuation and phase velocity of the plane and homogeneous waves are both frequency- and angle-dependent, as well as the anisotropy parameters (Thomsen 1986). From the elastic stiffnesses, complex P- and S-wave velocities of an equivalent VTI medium will be determined as a function of incident angle θ using the following formulation (e.g., Mavko et al. 2009).

$$v_{\text{P}} = \sqrt{\frac{\left(C_{11} + C_{44}\right)\sin^2\theta + \left(C_{33} + C_{44}\right)\cos^2\theta + \sqrt{D}}{2\rho}}, \tag{3}$$

$$v_{\text{SV}} = \sqrt{\frac{\left(C_{11} + C_{44}\right)\sin^2\theta + \left(C_{33} + C_{44}\right)\cos^2\theta - \sqrt{D}}{2\rho}}, \tag{4}$$

$$v_{\text{SH}} = \sqrt{\frac{C_{66}\sin^2\theta + C_{44}\cos^2\theta}{\rho}}, \tag{5}$$

$$\text{D} = \left[\left(C_{11} - C_{44}\right)\sin^2\theta - \left(C_{33} - C_{44}\right)\cos^2\theta\right]^2 + 4\left(C_{13} + C_{44}\right)^2\sin^2\theta\cos^2\theta. \tag{6}$$

Equations (3)-(6) are exact for an anisotropic VTI medium. In these equations, the bulk density is defined as $\rho = (1-\varphi_{\text{b}})\rho_{\text{s}} + \varphi_{\text{b}}\rho_{\text{f}}$, where φ_{b} is porosity of the background porous medium and ρ_{s} and ρ_{f} are grain and pore-fluid densities, respectively. Subsequently, we obtain the phase velocity and attenuation of the three wave modes as (Mavko et al. 2009).

$$V_i(\omega,\theta) = \left[\text{Re}\left(\frac{1}{v_i}\right)\right]^{-1} \tag{7}$$

$$Q_i^{-1}(\omega,\theta) = -\frac{\text{Im}\left(v_i^2\right)}{\text{Re}\left(v_i^2\right)} \tag{8}$$

where i indicates either the P-, the SV- or the SH-wave mode. Precise forms of the above relationships are also presented in Kong et al. (2017) and He et al. (2020).

To examine the influences of fracture-filled fluid variations on the phase velocity and seismic attenuation (or inverse quality Q^{-1}) behaviors, we consider a poroelastic sandstone with water saturation. The assumed fractured sandstone has 20% rock porosity and consists of quartz as the grain material (bulk modulus $K_{\text{g}} = 37$ GPa and density $\rho_{\text{g}} = 2650$ kg/m^3), which is adapted from Kong et al. (2017). The pore-fluid properties of water are density $\rho_{\text{f}} = 1000$ kg/m^3, viscosity $\eta_{\text{f}} = 10^{-3}$ Pa·s and bulk modulus $K_{\text{f}} = 2.25$ GPa. According to the proposed approach in Krief et al. (1990), the bulk and shear moduli of the dry background media can be estimated using the rock porosity with the following equation.

$$\frac{K_{\text{b}}}{K_{\text{s}}} = \frac{\mu_{\text{b}}}{\mu_{\text{s}}} = \left(1 - \varphi_{\text{b}}\right)^{3/(1-\varphi_{\text{b}})} \tag{9}$$

where K_{s} and μ_{s} are bulk and shear modulus of the grain, respectively. We set the fracture normal weakness $\delta_{\text{N}} = 0.2$. The dependence of rock permeability κ of the dry background medium on porosity is assumed to follow the empirical Kozeny–Carman relation.

$$\kappa = \frac{15\left(\varphi_{\text{b}} - 0.035\right)^3 100^2}{\left(1.035 - \varphi_{\text{b}}\right)^2} \tag{10}$$

In Fig. 1, the variations of phase velocity and inverse quality factor as functions of incident angle and frequency are demonstrated for the P- and SV-waves propagating in a fractured porous equivalent medium with pores and fractures filled by two different fluids. We observe apparent velocity dispersion and attenuation over the seismic exploration

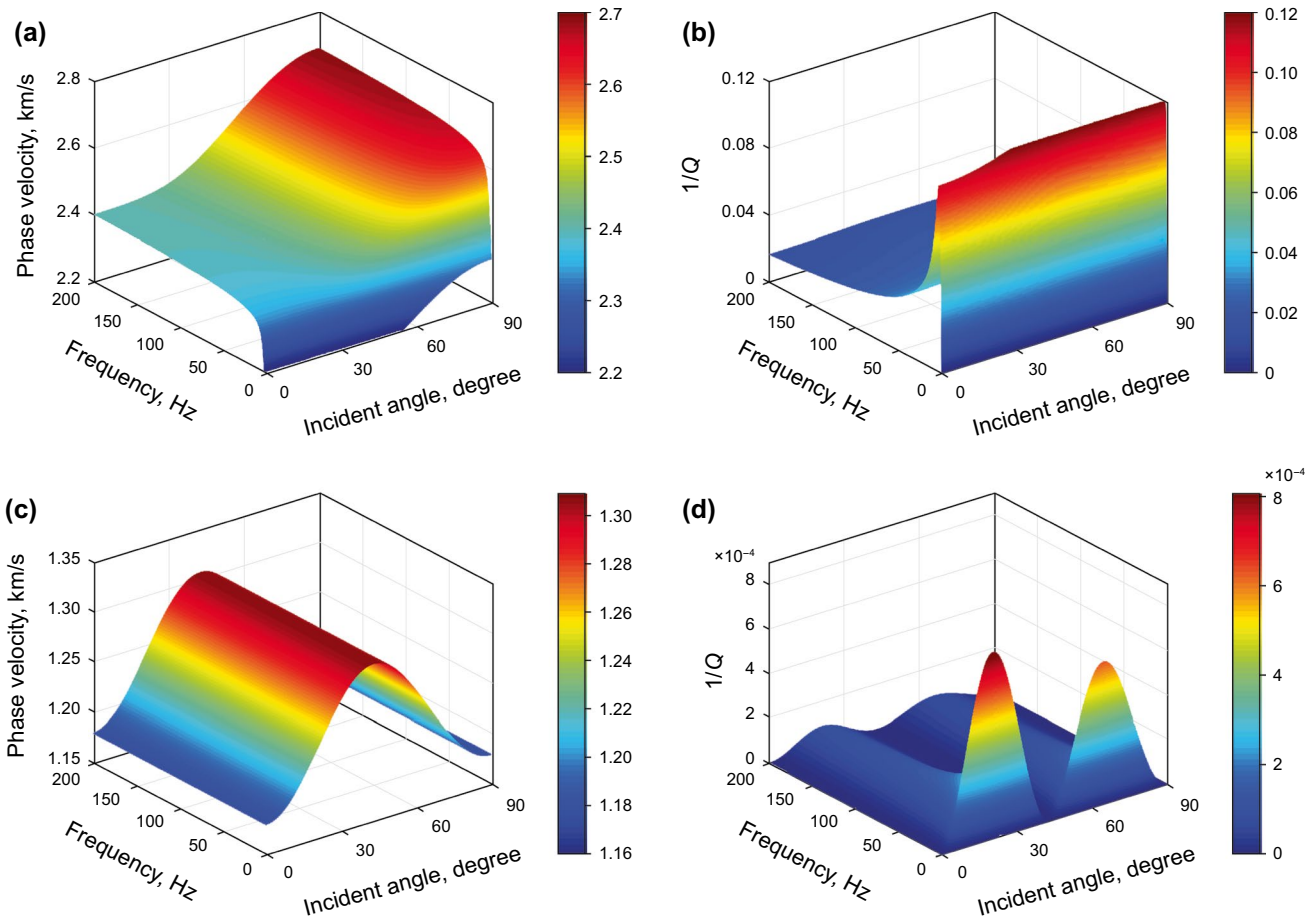

Fig. 1 Variations of the **a**, **c** phase velocities and the **b**, **d** inverse quality factors (Q^{-1}) with frequency and incident angle in a fractured porous medium, where pores and fractures are filled with two different fluids. In addition, graphs **a** and **b** correspond to the P-wave and, **c** and **d** correspond to the SV-wave, respectively

band. Please note attenuation of the SV-wave is quite small compared to that of the P-wave in the low frequencies.

In Fig. 2, the estimated phase velocity and attenuation of P- and SV-waves are displayed, respectively, for P- and SV-waves as functions of frequency and incident angle. In Fig. 2, velocity variations, as well as the maximum attenuation peaks, are very large for both liquid-filled ($F = 100$ corresponding to fracture fluid bulk modulus $K_{fc} = 16$ GPa) and nearly dry ($F = 0.01$ corresponding to highly compressible gases) fractures. The variations, nevertheless, become fairly smaller at intermediate values of the fracture fluid compressibility, particularly approaching zero when F is around the critical value F^*, at which there is no fluid low at all. Here, the dimensionless parameter F, which is associated with the fluid compressibility, is defined as the ratio of the bulk modulus of the fracture fluid (K_{fc}) and the dry P-wave modulus of fracture medium (L_c). We also find that all curves in Fig. 2 exhibit similar features of trends and shapes for both cases of incident angle $\theta = 0°$ and $\theta = 30°$. When the fluid compressibility of fracture is relatively small (i.e., $F > F^*$), we observe from Fig. 2(a) that the levels of P-wave velocity dispersion (differences between velocities at the high-limit and low-limit frequencies) at an incident angle of 30° are weaker than that at an incident angle of 0°. Nevertheless, when the fracture fluid compressibility is very large (i.e., $F < F^*$), we find slight variations between the magnitudes of velocity dispersion from incident angles of 0° and 30°. Meanwhile, we see the frequency-dependent SV-wave velocity and attenuation exhibits an apparent increase with increasing F values at 30° incident angle. Conversely, acoustic properties with a 0° incident angle show frequency independence for varying F values. Based on the numerical modeling results, we can draw a simple conclusion that wave attenuation (or inverse quality factor) and velocity dispersion always coexist and vary with incident angles, indicating an effect referred as frequency-dependent anisotropy.

Behaviors of the inverse quality factor and phase velocity variations with the incident angle and frequency can be characterized ulteriorly through examining the frequency-dependent anisotropy attributes, whose concise and apparent

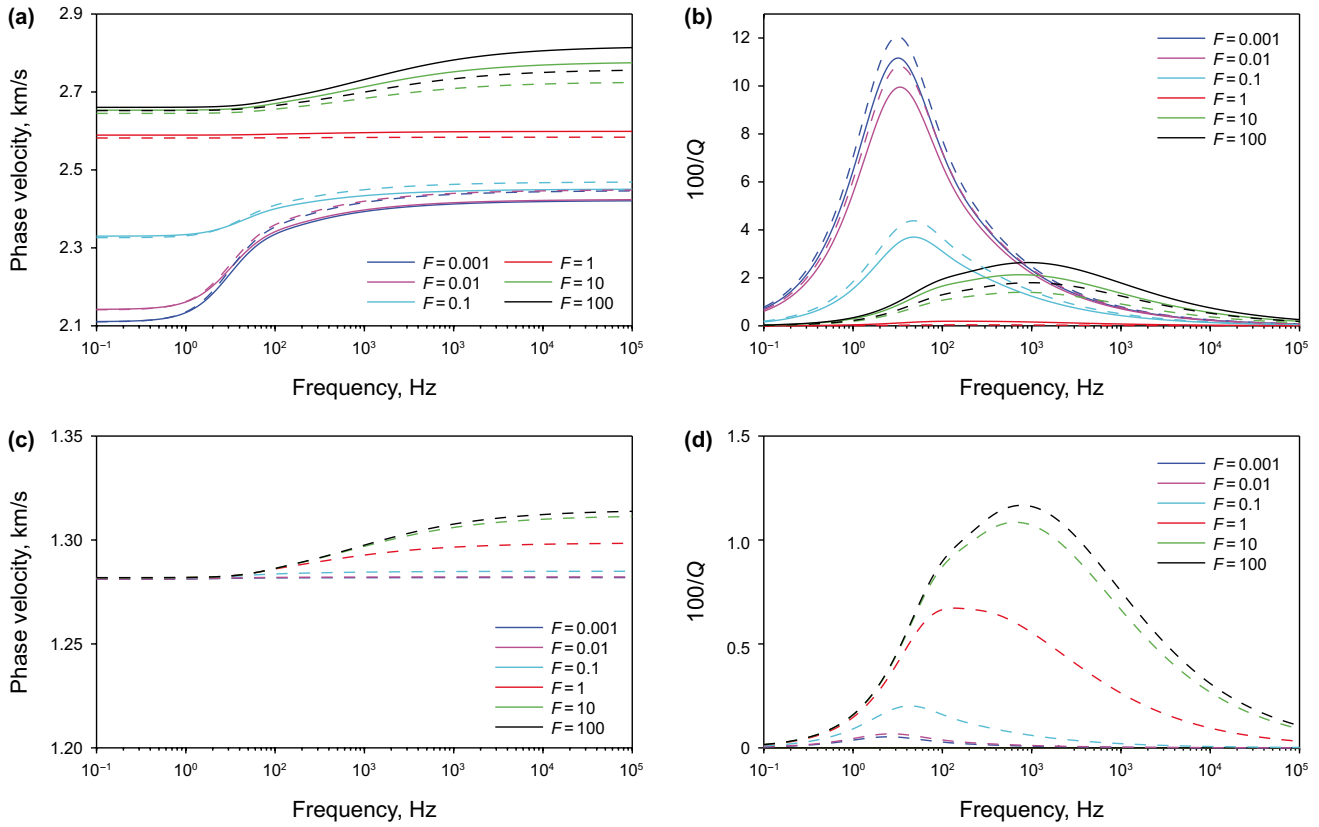

Fig. 2 Illustrations of the frequency dependence of **a**, **c** phase velocity and **b**, **d** scaled inverse quality factor (100/Q) of P-wave (top) and SV-wave (base) for different values of parameter F that indicates the fracture fluid compressibility. The dashed lines indicate the calculated acoustic properties with the incident angle 30° and solid lines with the incident angle 0°

expressions can be obtained by computing the frequency dependence of Thomsen's anisotropy parameters (Thomsen 1986). As the elastic stiffness coefficients are complex valued, the P-wave anisotropic parameters are also complex. Accordingly, the Thomsen's anisotropy parameter ε can be computed using (e.g., Thomsen 1986; Kong et al. 2017).

$$\varepsilon = \frac{C_{11} - C_{33}}{2C_{33}}. \tag{11}$$

Here, we refer the real and imaginary compartments of parameter ε as the respective phase velocity and attenuation anisotropy parameters. For the different values of F, Fig. 3 displays the frequency dependence characteristics of the real

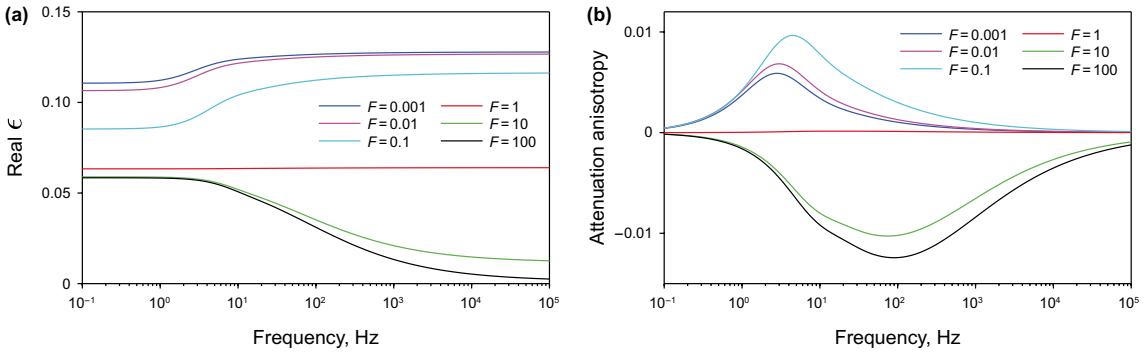

Fig. 3 Illustrations of frequency dependence of the **a** real compartment of the complex anisotropy parameter ε and the **b** alternative attenuation anisotropy parameter ε_Q for varying F values. In addition, note that different values of parameter F correspond to varied fracture fluid compressibility

and imaginary components for the complex parameter ε. In addition, we observe from Fig. 3 that parameters ε and ε_Q are separated into two distinct areas, corresponding to different F values. In Fig. 3a, we find that the pore pressure is equilibrated between pores and fractures, when fractures are filled with a very compressible fluid (i.e., gas) and $F > F^*$. Moreover, an alternative way to evaluate the magnitudes of wave attenuation is to use a dimensionless parameter $\varepsilon_Q = 1/Q_{33} - 1/Q_{11}$ (Galvin and Gurevich 2015). We can observe from Fig. 3b that parameter ε_Q tends to zero in the low- and high-frequency limits, and produces a peak magnitude in the intermediate frequencies for varied F values.

2.2 Frequency-dependent poroelastic seismic reflection coefficient

As illustrated in Figs. 1, 2 and 3, effective elastic stiffness tensors of the fluid-filled fractured porous sandstone reservoirs show significant incident angle and frequency dependence and, hence, will yield frequency- and angle-dependent characteristics of seismic AVO responses. In a poroelastic medium with stratified structures, seismic reflections embody the complex combined impacts of dynamic information regarding the impedance contrast across the interfaces, incident angles and interferences, as well as the anisotropy, velocity dispersion and attenuation of the viscoelastic reservoir. Hence, it is necessary to introduce an improved modeling scheme for calculating such complex seismic reflections using methods based on the conventional single interface reflection model methods (e.g., Chapman et al. 2006; Liu et al. 2011; Zhao et al. 2015).

We introduce a seamless procedure in this work that directly links rock physics modeling and seismic reflection computations on the basis of an extended propagator matrix method in Carcione (2001). The forward modeling algorithm can accurately allow in this improved workflow the frequency-dependent complex stiffnesses (anisotropic velocity and attenuation) predicted from rock physics modeling and yield angle- and frequency-dependent reflection coefficients and produce synthetic seismograms of a stratified model in the frequency and slowness domain. For a propagating P-wave with an incident angle θ, the corresponding reflection and transmission coefficients vector $R = [R_{PP}, R_{PS}, T_{PP}, T_{PS}]^T$ is written as (e.g., Carcione 2001).

$$R = -\left[A_1 - \left(\prod_{j=1}^{N} B_j\right) A_2\right]^{-1} i_p, \tag{12}$$

where A_1 and A_2 represent the propagation matrices associated with the rock elastic properties in the upper and lower media, B_j $(j = 1,..., N)$ represents the propagator matrix for the stratified media consisting of N thin beds, and i_P represents the P-wave incidence vector related to the elastic properties of the incident medium, respectively, which can be expressed by

$$i_P = i\omega\left[\beta_{P_1}, \gamma_{P_1}, -Z_{P_1}, -W_{P_1}\right]^T, \tag{13}$$

$$A_1 = i\omega\begin{pmatrix} \beta_{P_1} & \beta_{S_1} & 0 & 0 \\ -\gamma_{P_1} & -\gamma_{S_1} & 0 & 0 \\ -Z_{P_1} & -Z_{S_1} & 0 & 0 \\ W_{P_1} & W_{S_1} & 0 & 0 \end{pmatrix}, \tag{14}$$

$$A_2 = i\omega\begin{pmatrix} 0 & 0 & \beta_{P_2}\exp\left(-i\omega s_{Z_{P_2}} h\right) & \beta_{S_2}\exp\left(-i\omega s_{S_2} h\right) \\ 0 & 0 & \gamma_{P_2}\exp\left(-i\omega s_{Z_{P_2}} h\right) & \gamma_{S_2}\exp\left(-i\omega s_{Z_{S_2}} h\right) \\ 0 & 0 & -Z_{P_2}\exp\left(-i\omega s_{Z_{P_2}} h\right) & -Z_{S_2}\exp\left(-i\omega s_{Z_{S_2}} h\right) \\ 0 & 0 & -W_{P_2}\exp\left(-i\omega s_{Z_{P_2}} h\right) & -W_{S_2}\exp\left(-i\omega s_{Z_{S_2}} h\right) \end{pmatrix}, \tag{15}$$

$$B_j = T(0)T^{-1}(h_j), \tag{16}$$

where parameters W, Z, s_Z, β *and* γ with the scripts of P and S correspond to the quasi-longitude and shear waves, respectively; the subscripts 1 and 2 represent the upper and lower media; β and γ denote the horizontal and vertical complex polarization, respectively; h denotes the total layer thickness of the interbedded model ($\sum_{j=1}^{N} h_j$), with each of them having a thickness h_j. In addition, note that the above parameters are complex functions of incident wave frequency and slowness. In this case, the reflection and transmission coefficients are related to the elastic stiffness and incident angle, as well as the incident wave frequency, layer thickness and stratified structures of a reservoir.

According to Eqs. 12 to 16, angle- and frequency-dependent reflection coefficients are estimated for the fractured porous reservoir model having an interbedded structure. Sequentially, synthetic seismic waveforms can be yielded via multiplying the complex reflection coefficients R_{PP} and R_{PS} with the spectrum of an incident wavelet and then implementing inverse Fourier transform,

$$S_{PQ} = \frac{1}{2\pi}\int_{-\infty}^{\infty} W(\omega) R_{PG}(\theta;\omega) e^{i\omega t} \mathrm{d}\omega \tag{17}$$

where G denotes P- or SV-waves, and $W(\omega)$ represents the wavelet in frequency domain.

Here, on the basis of the proposed methodology of rock physics simulation and the propagator matrix approach, we simulate numerically and assess the effects of fracture infills (in liquid and gas phases) on frequency-dependent seismic AVO signatures of PP- and PS-waves in a fractured porous

model having significant wave attenuation, velocity dispersion and anisotropic properties, correspondingly.

3 Numerical modeling and analysis: seismic amplitude-versus-angle and frequency responses

3.1 Seismic response sensitivity to frequency-dependent anisotropy

We calculate the seismic responses for the models, in which an attenuative and dispersive sandstone reservoir is either overlaid by a shale half-space (model 1) or interbedded between two shale half-spaces (model 2), with only small differences in rock elasticities across the interface. In this study, we concentrate on assessing the impact of attenuative and dispersive elasticity anomalies of an effective VTI anisotropic medium on seismic reflection signatures, and thus the overburden shale is assumed to represent purely elastic and isotropic properties, whose P- and S-wave velocities are set to 3650 and 1830 m/s, respectively. Due to wave attenuation and velocity dispersion of the P- and S-waves, seismic reflection coefficients at the interface separating the nondispersive shale and the dispersive reservoir layer will be a function of the frequency and incident angle.

In Fig. 4, the magnitudes of the PP-wave reflection coefficient as a function of frequency and incident angle are demonstrated, along with the AVO curves extracted for the low- and high-frequency limits. PP reflection coefficients from the model 1 are shown in Fig. 4a for a dispersive sandstone layer, and in Fig. 4c for the sandstone with anisotropic velocity and attenuation predicted in Fig. 1. Within seismic exploration bands, we observe that seismic reflection coefficients of two cases show similar dependence characteristics on the frequency. Meanwhile, the class III AVO curves separate for the low- and high-frequency limits, while curves of the anisotropic model coincide at lager incident angle as displayed in Fig. 4b, d. The numerically modeling results also imply that the normal incidence reflection coefficients in the low-frequency bands are larger than that of the high-frequency band. Moreover, we observe in Fig. 4e, g that considering the existence of stratified structure drastically alters frequency-dependent AVO signatures for the isotropic and anisotropic cases. We also note that the absolute value of the reflection coefficient tends to increase and then decrease with increasing frequencies. This phenomenon indicates that the existence of the stratified structure may provide potential interpretations for reservoir hydrocarbon identifications. Accordingly, seismic AVO responses calculated at the low- and high-frequency limits show more complicated variations.

Although the simulated results apparently demonstrate how the seismic AVO behaviors can be affected by velocity dispersion and attenuation of the reservoir layer, evaluation of the reservoir anisotropy influences on seismic AVO responses is also important via considering the fractured reservoir as an equivalent VTI medium. In Fig. 5, the PP- and PS-wave reflection coefficients of models 1 and 2 are illustrated for the isotropic and anisotropic cases, respectively. Due to medium anisotropy, anomalies of AVO response tend to be more obvious than their equivalent isotropic case. These implications indicate that the presence of rock anisotropy can produce substantial impact on seismic AVO behaviors. In addition, the presence of layered structure results in more significant AVO response anomalies. And thus, it is necessary to consider rock anisotropy effects during seismic AVO analysis of fractured hydrocarbon-bearing reservoirs.

3.2 Layer thickness effect on frequency-dependent AVO signatures

We then explore the effect of varied reservoir layer thickness on the frequency-dependent seismic AVO response behaviors. Figures 6 and 7 illustrate the frequency dependence of computed reflection coefficients for the PP- and PS-waves, and the associated amplitude spectra and seismic waves for two cases of the interbedded reservoir with a layer thickness of 10 and 35 m, correspondingly. Here, to simulate the real petrophysical properties of the fractured porous reservoirs, we assume the sandstone medium exhibits significant attenuation and velocity dispersion versus each incident angle.

In Figs. 6a, b, 7a, b, we find that the layer thickness has an important influence in causing the frequency-dependent seismic AVO response anomalies. For the case of the interbedded sandstone with a layer thickness of 35 m, seismic reflection coefficients exhibit obvious oscillation with varying frequencies for each incident angle, and the period of the oscillation increases with the increasing incident angle. Meanwhile, we also obtain the reflection amplitude spectra, through multiplying frequency-dependent reflection coefficients with the spectrum of a source Ricker wavelet with the peak frequency of 30 Hz. Additionally, we observe from Figs. 6 and 7 that the reflection amplitudes present marked behaviors of variations with incident angle for both the interbedded reservoirs with the layer thicknesses of 10 m and 35 m, respectively. It is also interesting to find that the energy of reflected waves from the reservoir of 35 m layered thickness is larger than that from the reservoir with a 10 m thickness, and reflections for the two models show two different types of AVO behaviors.

Through applying the inverse Fourier transform for reflection amplitude spectra, we obtain seismic waveforms of PP- and PS-waves, respectively. Here, we can observe that the synthetic waveforms become more complex at large angle

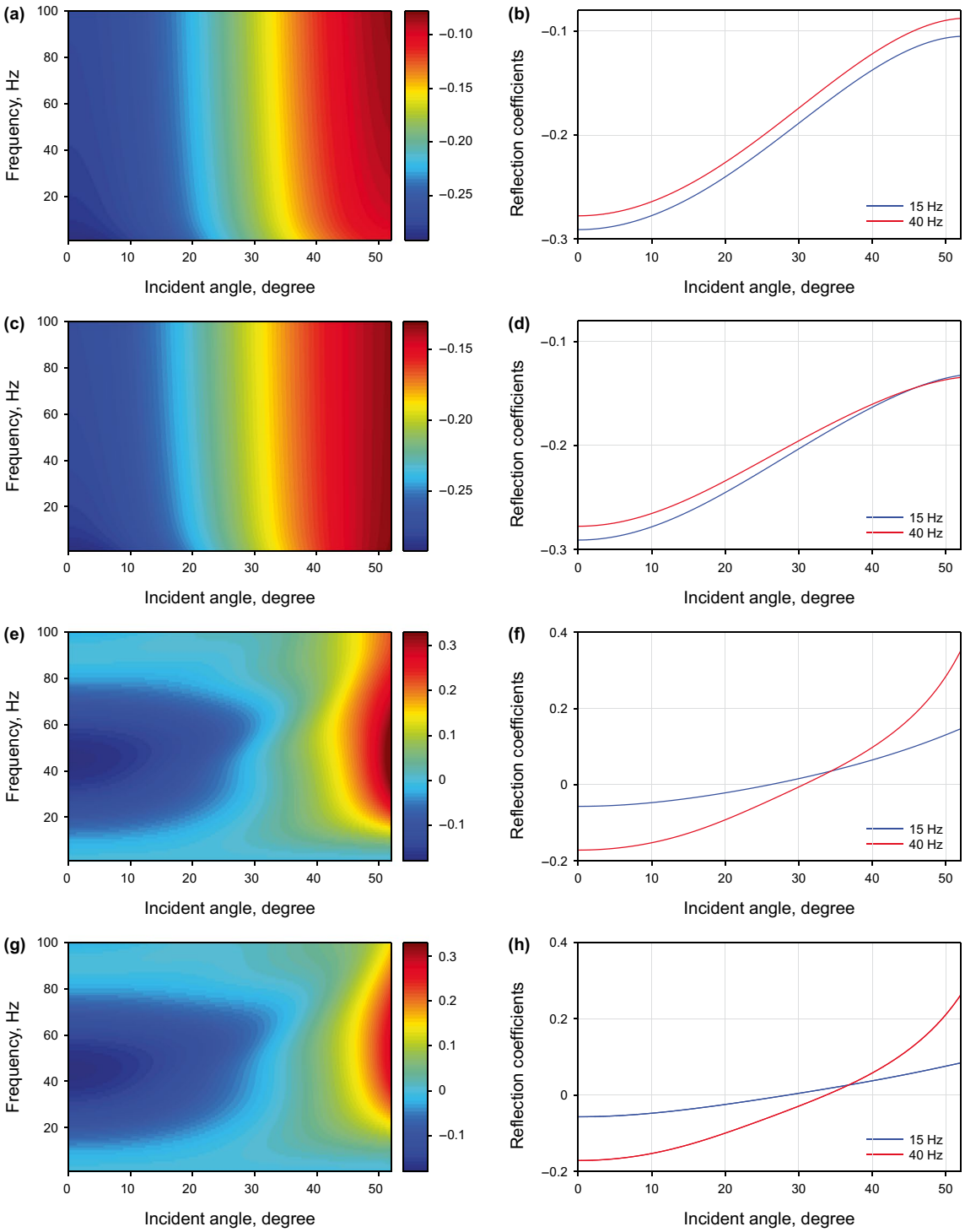

Fig. 4 Estimated (left column) PP-wave reflection coefficients and the (right column) corresponding AVO curves extracted for the low- and high-frequency limits are illustrated. **a** represents the dispersive case of a sandstone half-space, **c** represents anisotropic and dispersive sandstone half-space, **e** represents layered and dispersive sandstone with a thickness of 15 m, and **g** represents the corresponding model to **e** but considering medium anisotropy effects. Colors: the blue lines correspond to the low-frequency limit of 15 Hz, while red lines correspond to the high-frequency limit of 40 Hz

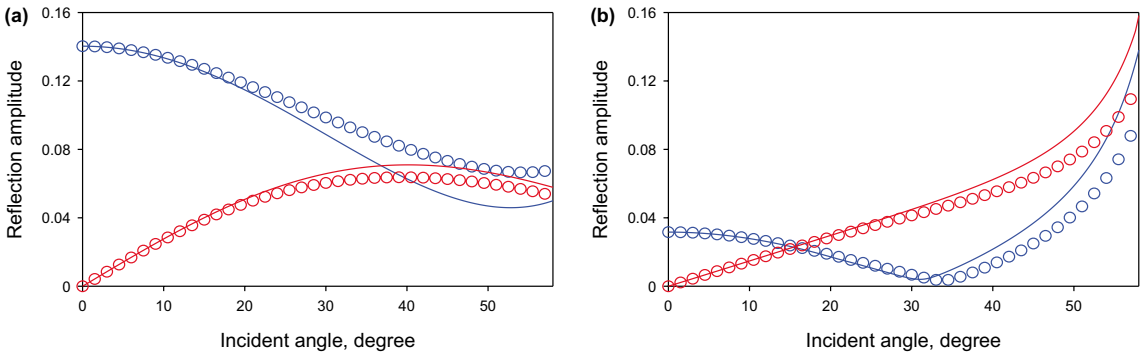

Fig. 5 Variations of the reflection coefficient as a function of incident angle, corresponding to the (solid lines) isotropic and (hollow circles) anisotropic cases for the **a** anisotropic and dispersive sandstone half-space, and the **b** layered and anisotropic sandstone reservoir with a layer thickness of 15 m. In addition, the blue curves represent PP-wave and the red represent PS-wave

of incident waves. It is interesting to observe from Fig. 7c that reflections from the top interface of the thick reservoir layer show the typical class III AVO behaviors. Reflected wavetrains at the bottom reservoir interface, nevertheless, represent a combining contribution of the elastic impedances, velocity dispersion and attenuation of the anisotropic reservoir, layer thickness and incident angle. These numerical results reveal that it is inappropriate to treat the bottom interface reflection as a typical AVO response. Moreover, for the thinner reservoir in Fig. 6c, the seismic reflections embody the combined effects regarding velocity dispersion and attenuation within the fractured reservoir, as well as the tuning and interference reflections. In this case, thus, it would be more appropriate to study seismic responses of the fractured porous reservoir in terms of the integrated reflection waveforms rather than from the viewpoint of the reflected waves at the top and bottom reservoir interfaces, respectively.

3.3 Effects of fracture infill on frequency-dependent seismic reflection signatures

An effective fractured VTI medium that is saturated with two different fluids can cause varied frequency and angle dependence values of the phase velocity and quality factor, hence resulting in distinct seismic AVO response anomalies. To demonstrate the impact of fracture infills on frequency-dependent seismic reflection signatures, we calculate seismic reflection coefficients and the corresponding waveform responses for a fractured porous sandstone with varied fracture fluids (i.e., different F values here). Via assuming a stratified model in which the viscoelastic reservoir is sandwiched between two elastic isotropic half-spaces, we concentrate on seismic response anomalies associated with frequency-dependent anisotropic dispersion and attenuation of the reservoir layer, as well as the stratified structure.

In Fig. 8a, b, the predicted amplitude spectra of PP reflections, where apparent derivations existing in terms of bandwidth, energy and amplitude variation with incident angel are frequency, are illustrated for the models with fractures filled by liquid and gas, respectively. Correspondingly, the synthetic waveforms in Fig. 8c, d show differences in the waveform and AVO behaviors. Nevertheless, the PS-wave reflected waveforms for the models with fractures filled by liquid and gas exhibit insignificant deviations, as shown in Fig. 9. These modeling results imply that it can be challenging to accurately discriminate seismic reflection signature alternations induced by fracture infill variations using the PS-wave reflections solely.

3.4 Impacts of fracture weakness on frequency-dependent seismic reflection signature variations

According to previous studies that the magnitude of wave attenuation and velocity dispersion relies significantly on the degree of fracturing of a porous medium (e.g., Chapman et al. 2003; Brajanovski et al. 2005), and we consider in this work the effect of fracture weakness of the porous sandstone on frequency-dependent seismic AVO signatures.

In Fig. 10, the seismic amplitude spectra and synthetic waveforms of PS-wave reflections from the single-layer interbedded model, corresponding to different fracture weaknesses, are demonstrated via assuming the fractured porous sandstone reservoir with a 30 m thickness. We see

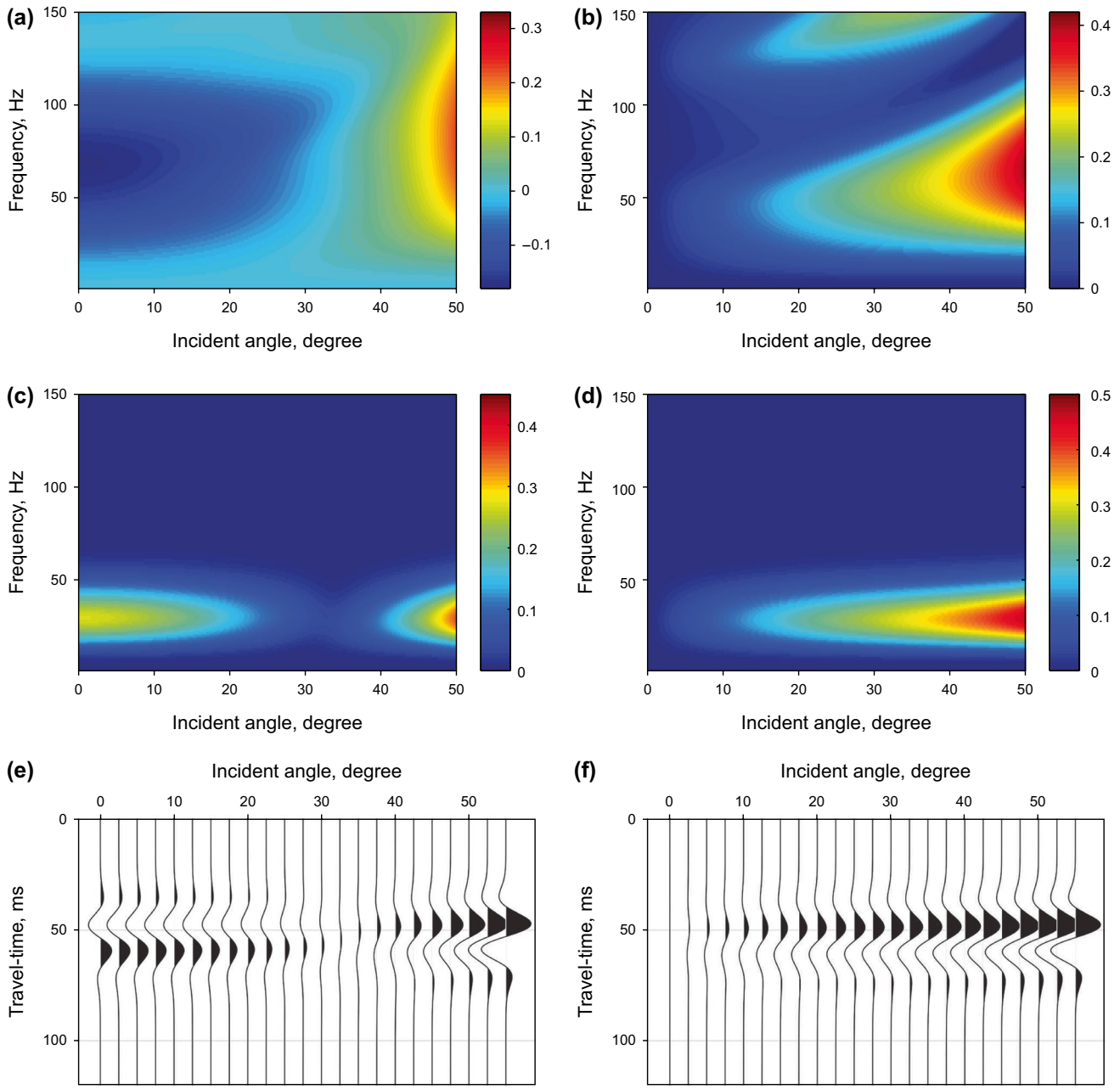

Fig. 6 Illustrations of **a**, **b** the frequency-dependent reflection coefficients, **c**, **d** the amplitude spectra and **e**, **f** the associated seismograms of (left column) PP- and (right column) PS-waves, respectively. The interbedded poroelastic sandstone layer having a thickness of 10 m is saturated by two different fluids with corresponding medium anisotropy and velocity dispersion

that apparent variations exist in energy, time and waveforms between the two fracturing cases. Meanwhile, seismic amplitudes of the spectra from the fractured layer with fracture weakness $\delta_N = 0.1$ are larger than those from the sandstone with $\delta_N = 0.01$. Correspondingly, synthetic seismograms of the PP-wave reflections in Fig. 11 exhibit obviously influences of wave attenuation and velocity dispersion of the fractured porous reservoir, particularly for the base reservoir reflections that are further complicated by waves traveling through the dispersive and attenuative sandstone layer. In addition, the fracture tangential weakness δ_T levels varying

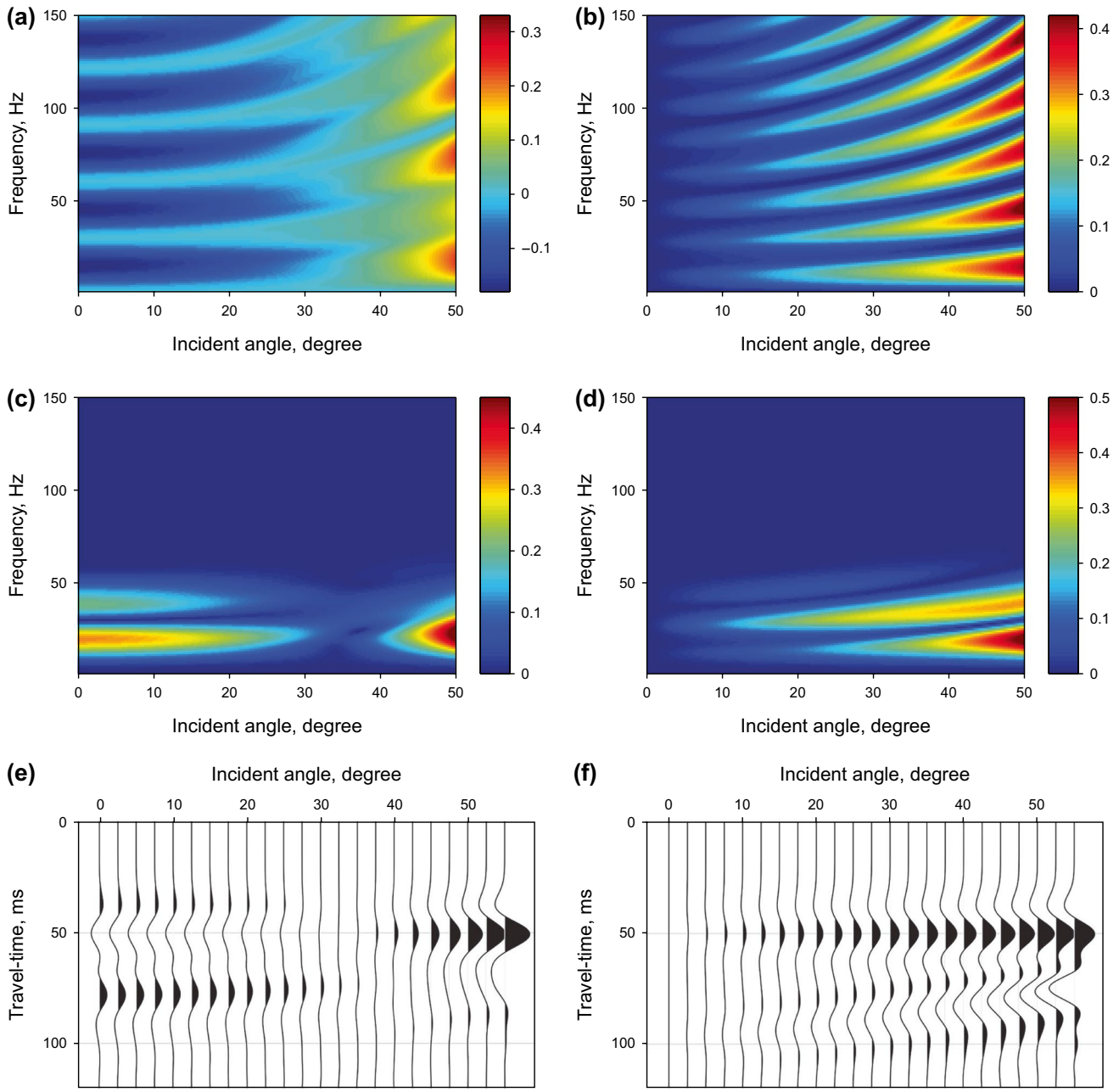

Fig. 7 Illustrations of **a**, **b** the frequency-dependent reflection coefficients, **c**, **d** the amplitude spectra and **e**, **f** the associated seismograms for (left column) PP- and (right column) PS-waves for the model in Fig. 6, for which the porous sandstone reservoir has a layer thickness of 35 m

from 0 and 1 have also an important impact on the predicted complex stiffness tensors, hence resulting in abnormal reflection coefficient variations. Sensitivity of fracture tangential weakness to the acoustic properties will be examined in a further study.

4 Conclusion

We have introduced an improved seismic AVO modeling method in this work to calculate frequency- and incident-angle-dependent reflection coefficients. The numerically modeling method allows linking the propagator matrix algorithm in the frequency domain and the rock physics simulation that can predict frequency-dependent anisotropic elastic stiffness tensors. Based on the modified methodology, we obtain the frequency-dependent PP- and PS-wave reflection

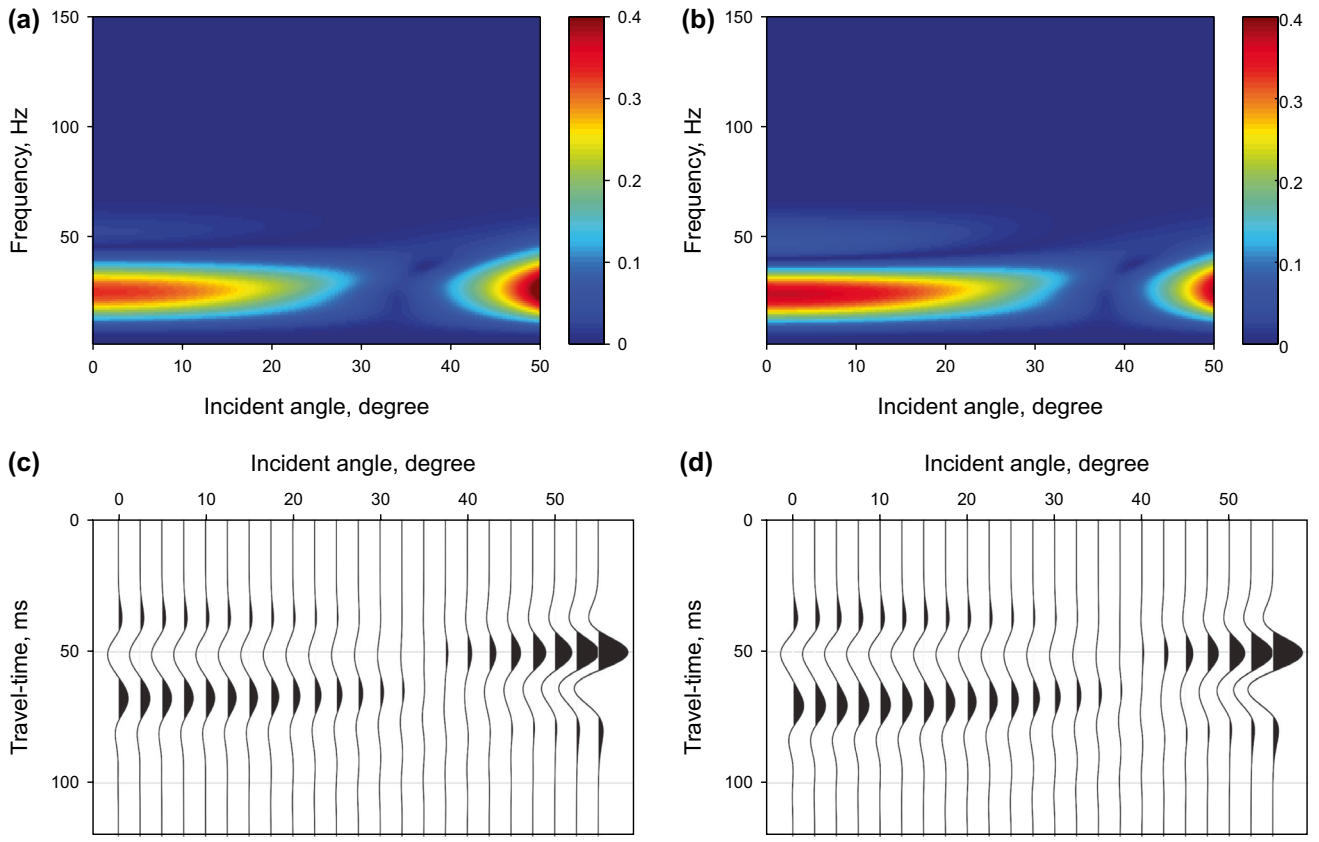

Fig. 8 Illustrations of the **a**, **b** PP-wave reflection amplitude spectra, and the **c**, **d** associated seismograms for the interbedded sandstone of 30 m layer thickness in Fig. 4**g** with fractures filled by liquid **a**, **c** and gas **b**, **d**, respectively

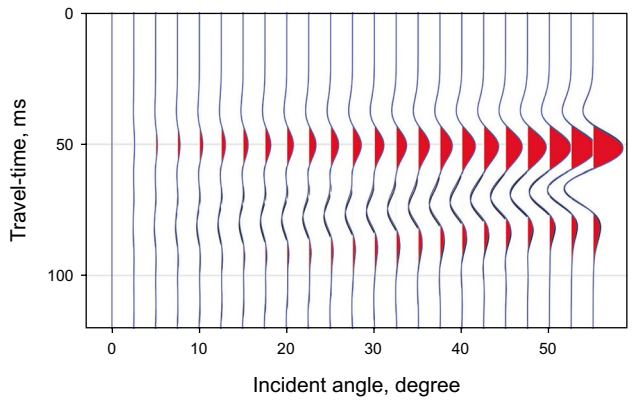

Fig. 9 Obtained seismograms of PS-wave reflections, corresponding to the layered sandstone model in Fig. 8. Here, the black trace corresponds to fractures filled with liquid and the red trace corresponds to gas-filled fractures, respectively

coefficients and the corresponding synthetic seismograms from an interbedded model with a porous sandstone layer containing sets of aligned fractures. In particular, we explore seismic attenuation and velocity dispersion variations of the fractured media. We have also illustrated the sensitivity of the seismic AVO anomalies to rock elastic properties, anisotropy, velocity dispersion and attenuation, and the layered structure, which cannot be studied using either normal-incident reflection technique or the conventional Zoeppritz equation-based interface reflection model algorithm. Numerical results of this study also indicate the feasibility of the modified frequency-dependent seismic AVO analysis approach for the detection of fracture infills, as well as the degree of fracturing, in a stratified reservoir system. The extended research may allow various kinds of effective media which can be determined using varied rock physics theories in the

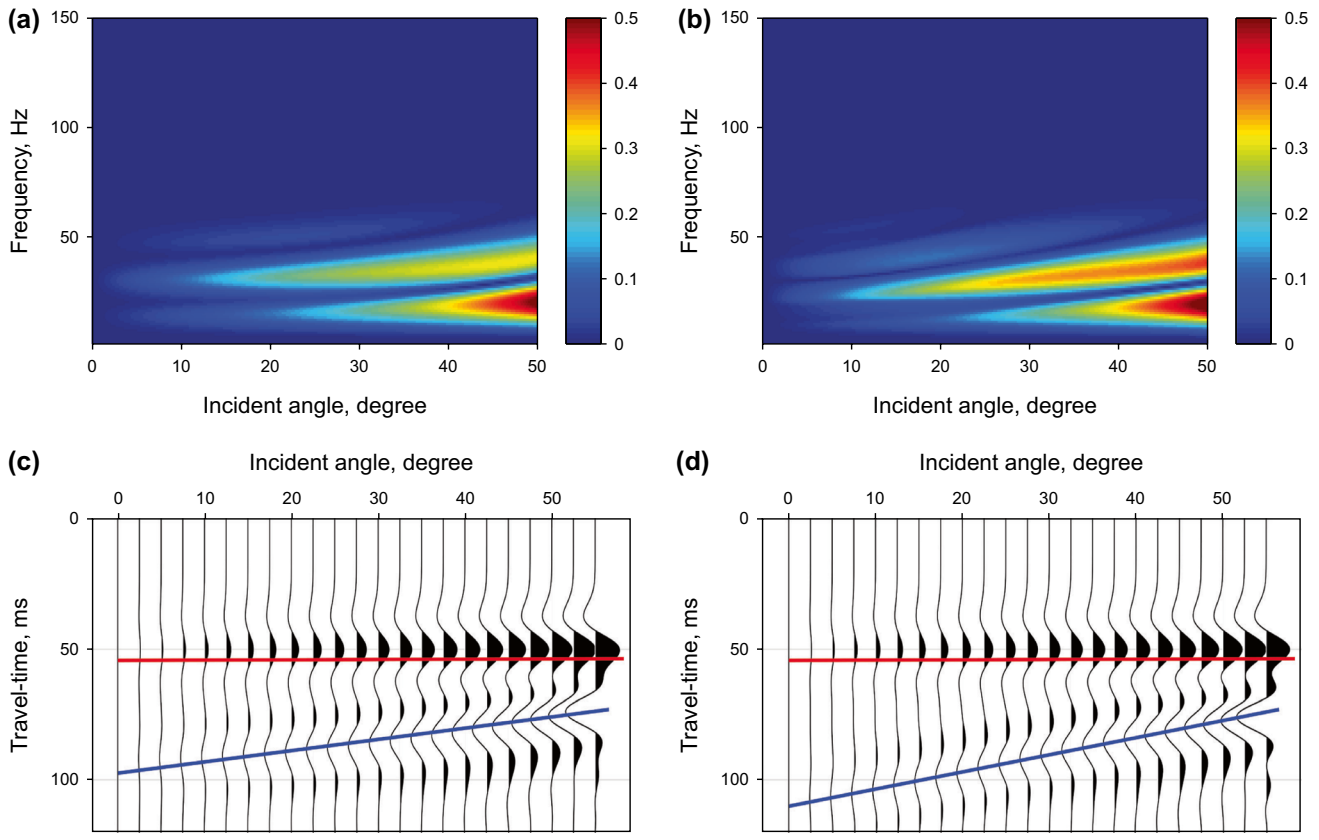

Fig. 10 Illustrations of the **a**, **b** PS-wave reflection amplitude spectra and the **c**, **d** associated seismic waveforms obtained using a 30 Hz Ricker wavelet, for the interbedded sandstone reservoir model of 30 m layer thickness in Fig. 1g. The fractured layer is saturated with two different fluids and has dry fracture normal weakness of **a**, **c** $\delta_N = 0.01$ and **b**, **d** $\delta_N = 0.1$, respectively

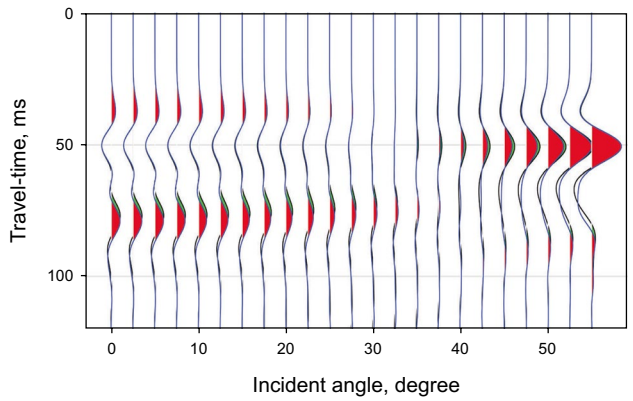

Fig. 11 Illustration of synthetic seismic waveforms of PP-wave reflections, corresponding to the interbedded sandstone reservoir model of 30 m layer thickness in Fig. 10. In addition, the fractured layer is saturated with two different fluids and has dry fracture normal weakness of (green) $\delta_N = 0.01$ and (red) $\delta_N = 0.1$, respectively

same model, such as to explore frequency-dependent seismic AVO signatures of a stratified system with more complex lithology and yield more accurate predictions of fracture fluids in a heterogeneously fractured reservoir.

Acknowledgements This work was financially supported by the Science Foundation of China University of Petroleum (Beijing) (2462020YXZZ008), the National Natural Science Foundation of China (41804104, 41930425, U19B6003-04-03, 41774143), the National Key R&D Program of China (2018YFA0702504), the PetroChina Innovation Foundation (2018D-5007-0303) and the Science Foundation of SINOPEC Key Laboratory of Geophysics (33550006-20-ZC0699-0001). The authors are grateful to the four anonymous reviewers, for their constructive comments and suggestions.

References

Biot MA. Mechanics of deformation and acoustic propagation in porous media. J Appl Phys. 1962;33(4):1482–98. https://doi.org/10.1063/1.1728759.

Brajanovski M, Gurevich B, Schoenberg M. A model for P-wave attenuation and dispersion in a porous medium permeated by aligned fractures. Geophy J Int. 2005;163(1):372–84. https://doi.org/10.1111/j.1365-246X.2005.02722.x.

Brajanovski M, Müller TM, Parra JO. A model for strong attenuation and dispersion of seismic P-waves in a partially saturated fractured reservoir. Sci China-Earth Phys Mech Astro. 2010;53(8):1383–7. https://doi.org/10.1007/s11433-010-3205-0.

Cao CH, Fu LY, Ba J, Zhang Y. Frequency- and incident-angle-dependent P-wave properties influenced by dynamic stress interactions in fractured porous media. Geophysics. 2019;84(5):MR173–84. https://doi.org/10.1190/GEO2018-0103.1.

Cao CH, Zhang HB, Pan YX, Teng XB. Relationship between the transition frequency of local fluid flow and the peak frequency of attenuation. Appl Geophys. 2016;13(1):156–65. https://doi.org/10.1007/s11770-016-0528-2.

Carcione JM. AVO effects of a hydrocarbon source-rock layer. Geophysics. 2001;66:419–27. https://doi.org/10.1190/1.1444933.

Carcione JM, Gurevich B, Santos JE, Picotti S. Angular and frequency-dependent wave velocity in fractured porous media. Pure Appl Geophys. 2013;170(1):1673–83. https://doi.org/10.1007/s00024-012-0636-8.

Carcione JM, Picotti S. P-wave seismic attenuation by slow-wave diffusion: Effects of inhomogeneous rock properties. Geophysics. 2006;71(3):O1–8. https://doi.org/10.1190/1.2194512.

Chapman M. Frequency dependent anisotropy due to meso-scale fractures in the presence of equant porosity. Geophys Prospect. 2003;51:369–79. https://doi.org/10.1046/j.1365-2478.2003.00384.x.

Chapman M, Liu ER, Li XY. The influence of fluid-sensitive dispersion and attenuation on AVO analysis. Geophy J Int. 2006;167(1):89–105. https://doi.org/10.1111/j.1365-246X.2006.02919.x.

Chichinina T, Sabinin V, Ronquillo-Jarillo G. QVOA analysis: P-wave attenuation anisotropy for fracture characterization. Geophysics. 2006;71:C37–48. https://doi.org/10.1190/1.2194531.

Deng JX, Zhou H, Wang H, Zhao JG, Wang SX. The influence of pore structure in reservoir sandstone on dispersion properties of elastic waves. Chinese J Geophys. 2020;58(9):3389–400. https://doi.org/10.6038/cjg20150931.**(in Chinese)**.

Dupuy B, Stovas A. Influence of frequency and saturation on AVO attributes for patchy saturated rocks. Geophysics. 2014;79(1):B19–36. https://doi.org/10.1190/GEO2012-0518.1.

Galvin RJ, Gurevich B. Frequency dependent anisotropy of porous rocks with aligned fractures. Geophys Prospect. 2015;63:141–50. https://doi.org/10.1111/1365-2478.12177.

Guo JX, Han T, Fu LY, Xu D, Fang X. Effective elastic properties of rocks with transversely isotropic background permeated by aligned penny-shaped cracks. J Geophys Res Sol Ea. 2019;124:400–42. https://doi.org/10.1029/2018JB016412.

Guo JX, Rubino JG, Barbosa ND, Glubokovskikh S, Gurevich B. Seismic dispersion and attenuation in saturated porous rocks with aligned fractures of finite thickness: Theory and numerical simulations—Part 1: P-wave perpendicular to the fracture plane. Geophysics. 2018;83:WA49–62. https://doi.org/10.1190/GEO2017-0065.1.

Guo ZQ, Liu C, Li XY. Seismic signatures of reservoir permeability based on the patchy-saturation model. Appl Geophys. 2015;12:187–98. https://doi.org/10.1007/s11770-015-0480-6.

Guo ZQ, Liu C, Liu XW, Dong N, Liu YW. Research on anisotropy of shale oil reservoir based on rock physics model. Appl Geophys. 2016;13(2):382–92. https://doi.org/10.1007/s11770-016-0554-0.

Guo ZQ, Liu XW, Fu W, Li XY. Modeling and analysis of azimuthal AVO responses from a viscoelastic anisotropic reflector. Appl Geophys. 2015;12:441–52. https://doi.org/10.1007/s11770-015-0498-9.

Guo ZQ, Li XY. Azimuthal AVO signatures of fractured poroelastic sandstone layers. Explor Geophys. 2017;48:56–66. https://doi.org/10.1071/EG15050.

Gurevich B, Makarynska D, de Paula OB, Pervukhina M. A simple model for squirt-flow dispersion and attenuation in fluid-saturated granular rocks. Geophysics. 2010;75:N109–20. https://doi.org/10.1190/1.3509782.

He YX, Wang SX, Wu XY, Xi B. Influence of frequency-dependent anisotropy on seismic amplitude-versus-offset signatures for fractured poroelastic rocks. Geophys Prospect. 2020;68:2141–63. https://doi.org/10.1111/1365-2478.12981.

He YX, Wu XY, Fu K, Zhou D, Wang SX. Modeling the effect of microscopic and mesoscopic heterogeneity on frequency-dependent attenuation and seismic signatures. IEEE Geosci Remote S L. 2018;15:1174–8. https://doi.org/10.1109/LGRS.2018.2829837.

He YX, Wu XY, Wang SX, Zhao JG. Reflection dispersion signatures due to wave-induced pressure diffusion in heterogeneous poroelastic media. Explor Geophysics. 2019;50(5):541–53.

Jin ZY, Chapman M, Papageorgiou G, Wu XY. Impact of frequency-dependent anisotropy on azimuthal P-wave reflections. J Geophys Eng. 2018;15:2530–44. https://doi.org/10.1088/1742-2140/aad882.

Kong LY, Gurevich B, Zhang Y, Wang YB. Effect of fracture fill on frequency-dependent anisotropy of fractured porous rocks. Geophys Prospect. 2017;65:1649–61.

Krief M, Garat J, Stellingwerff J, Ventre J. A petrophysical interpretation using the velocities of P and S waves (full-waveform sonic). Log Anal. 1990;31:355–69.

Krzikalla F, Muller TM. Anisotropic P-SV-wave dispersion and attenuation due to inter-layer flow in thinly layered porous rocks. Geophysics. 2011;76(3):WA135–45. https://doi.org/10.1190/1.3555077.

Kudarova AM, van Dalen KN, Drijkoningen GG. Effective poroelastic model for one-dimensional wave propagation in periodically layered media. Geophy J Int. 2013;195:1337–50. https://doi.org/10.1093/gji/ggt315.

Kumar M, Kumari M, Barak MS. Reflection of plane seismic waves at the surface of double-porosity dual-permeability materials. Pet Sci. 2018;15(3):521–37. .

Kumari M, Barak MS, Kumari M. Seismic reflection and transmission coefficients of a single layer sandwiched between two dissimilar poroelastic solids. Pet Sci. 2017;14(4):676–93. https://doi.org/10.1007/s12182-017-0195-9.

Li C, Zhao JG, Wang HB, Pan JG, Long T, Deng JX, Li Z. Multi-frequency rock physics measurements and dispersion analysis on tight carbonate rocks. Chinese J Geophys. 2020;63(2):627–37. https://doi.org/10.6038/cjg2019M0294.**(in Chinese).**

Liu LF, Cao SY, Wang L. Poroelastic analysis of frequency-dependent amplitude-versus-offset variations. Geophysics. 2011;76:C31–40. https://doi.org/10.1190/1.3552702.

Maultzsch S, Chapman M, Liu ER, Li XY. Modelling frequency-dependent seismic anisotropy in fluid-saturated rock with aligned fractures: implication of fracture size estimation from anisotropic measurements. Geophys Prospect. 2003;51:381–92. https://doi.org/10.1046/j.1365-2478.2003.00386.x.

Mavko G, Mukerji T, Dvorkin J. The rock physics handbook: Tools for Seismic Analysis of Porous Media. Cambridge: Cambridge Univ. Press; 2009.

Norris AN. Low-frequency dispersion and attenuation partially saturated rocks. J Acoust Soc Am. 1993a;94:359–70. https://doi.org/10.1121/1.407101.

Ren HT, Goloshubin G, Hilterman FJ. Poroelastic analysis of amplitude-versus-frequency variation. Geophysics. 2009;74(6):N41–8. https://doi.org/10.1190/1.3207863.

Rubino JGE, Caspari E, Müller TM, Milani M, Barbosa ND, Holliger K. Numerical upscaling in 2-D heterogeneous poroelastic rocks: Anisotropic attenuation and dispersion of seismic waves. J Geophys Res-Sol Ea. 2016;121:6698–721. https://doi.org/10.1002/2016JB013165.

Rubino JG, Holliger K. Research note: Seismic attenuation due to wave-induced fluid flow at microscopic and mesoscopic scales. Geophys Prospect. 2013;61:882–9. https://doi.org/10.1111/1365-2478.12009.

Rüger A. P-wave reflection coefficients for transversely isotropic model with vertical and horizontal axis of symmetry. Geophysics. 1997;62:713–22. https://doi.org/10.1190/1.1444181.

Shi P, Angus D, Nowacki A, Yuan S, Wang Y. Microseismic full waveform modeling in anisotropic media with moment tensor implementation. Surv Geophys. 2018;39(4):567–611. https://doi.org/10.1007/s10712-018-9466-2.

Tang XM. A unified theory for elastic wave propagation through porous media containing cracks-An extension of Biot's poroelastic wave theory. Sci China-Earth Sci. 2011;54(9):1441–52. https://doi.org/10.1007/s11430-011-4245-7.

Thomsen L. Weak elastic anisotropy. Geophysics. 1986a;51(10):1954–66. https://doi.org/10.1190/1.1442051.

Wu GC, Wu JL, Zong ZY. The attenuation of P-wave in a periodic layered porous media containing cracks. Chinese J Geophys. 2014;57(8):2666–77. https://doi.org/10.6038/cjg20140825. **(in Chinese)**.

Yang XH, Cao SY, Guo QS, Yu KYG, PF, Hu W. . Frequency-dependent amplitude versus offset variations in porous rocks with aligned fractures. Pure Appl Geophys. 2017;174:1043–59. https://doi.org/10.1007/s00024-016-1423-8.

Zhang GZ, He F, Zhang JJ, Pei ZL, Song JJ, Yin XY. Velocity dispersion and attenuation at microscopic and mesoscopic wave-induced fluid flow. OGP. 2017;52(4):743–51. https://doi.org/10.13810/j.cnki.issn.1000-7210.2017.04.012. **(in Chinese)**.

Zhang JW, Huang HD, Wu Ch, Zhang S, Wu G, Chen F. Influence of patchy saturation on seismic dispersion and attenuation in fractured porous media. Geophy J Int. 2018;214:583–95. https://doi.org/10.1093/gji/ggy160.

Zhao LX, Han DH, Yao QL, Zhou R, Yan FY. Seismic reflection dispersion due to wave-induced fluid flow in heterogeneous reservoir rocks. Geophysics. 2015;80(3):D221–35. https://doi.org/10.1190/GEO2014-0307.1.